JTTEE5 14:23-30
DOI: 10.1361/10599630522693
1059-9630/$19.00 © ASM International

Synthesis and Oxidation Behavior of Nanocrystalline MCrAlY Bond Coatings

Leonardo Ajdelsztajn, Feng Tang, George E. Kim, Virgil Provenzano, and Julie M. Schoenung

(Submitted July 28, 2003; in revised form December 16, 2003)

Thermal barrier coating systems protect turbine blades against high-temperature corrosion and oxidation. They consist of a metal bond coat (MCrAlY, M = Ni, Co) and a ceramic top layer (ZrO_2/Y_2O_3). In this work, the oxidation behavior of conventional and nanostructured high-velocity oxyfuel (HVOF) NiCrAlY coatings has been compared. Commercially available NiCrAlY powder was mechanically cryomilled and HVOF sprayed on a nickel alloy foil to form a nanocrystalline coating. Freestanding bodies of conventional and nanostructured HVOF NiCrAlY coatings were oxidized at 1000 °C for different time periods to form the thermally grown oxide layer. The experiments show an improvement in oxidation resistance in the nanostructured coating when compared with that of the conventional one. The observed behavior is a result of the formation of a continuous Al_2O_3 layer on the surface of the nanostructured HVOF NiCrAlY coating. This layer protects the coating from further oxidation and avoids the formation of mixed oxide protrusions present in the conventional coating.

Keywords high-velocity oxyfuel, MCrAlY, nanocrystalline coatings, oxidation behavior

1. Introduction

In gas turbine engines, higher efficiency can be achieved by increasing the operating temperature. Hot section components such as combustors, blades, and vanes are generally made from nickel-based superalloys. The operating temperature of these alloys is generally limited to less than 1000 °C (Ref 1), and it can be increased if a thermal insulation layer is applied to the hot surfaces. A powerful approach to achieve a thermal insulation layer is to apply thermal barrier coatings (TBCs) onto the hot surfaces (Ref 2-4). Thermal barrier coatings are capable of increasing the operating temperatures by as much as 200 °C (Ref 5), and present engine-operating temperatures, for some specific applications, are in the 1000 to 1150 °C range. At those temperatures, the TBCs also provide protection to the Ni-based superalloys against high-temperature oxidation and hot corrosion attack.

The TBCs applied on Ni superalloys consist of a ceramic topcoat (ZrO_2/Y_2O_3) and a metallic bond coat (MCrAlY, M = Ni, Co or both) (Ref 6). The porous topcoat, which is bonded to the bulk material via the bond coat, can protect the underlying air-cooled material by significantly reducing its operating temperature. The metallic bond coat serves also to protect the bulk material from corrosion and oxidation. Conventional commercial MCrAlY coatings have compositions containing: 18 to 30 wt.% Cr, 5 to 14 wt.% Al, 0.5 to 1.5 wt.% Y, and balance Ni, Co, or Ni and Co to provide the best balance between optimal corrosion protection and high-temperature oxidation resistance (Ref 7).

Although the TBC technique was developed for turbine engines over two decades ago, the premature failure of TBCs during thermal cycling is still a critical problem, which severely limits the lifetime of the coated components. This premature failure of TBCs is usually caused by the spallation of the topcoat, which is mostly due to the thermomechanical fatigue cracking along or close to the interface between the bond coat and the topcoat (Ref 8, 9). The cracking is believed to be related to the thickness and nature of the thermally grown oxide (TGO) layer, which is formed at the interface between the bond coat and the topcoat as a result of the reaction between the oxygen penetrating through the topcoat and the metallic elements from the bond coat. Therefore, the modification of oxidation behavior in the bond coat is very important in improving the lifetime of TBCs.

In recent efforts to increase the efficiency of gas turbine engines and the lifetimes of high-temperature-resistant components, the composition of the MCrAlY coatings, together with the variation in grain size, have been studied by Liu et al. (Ref 10, 11). These researchers have used magnetron-sputtering deposition (MSD) to study the effect of the composition and grain size of the constituents on the oxidation behavior of NiCrAl coatings. The MSD provides an effective way of producing fine-grained materials. The results of the studies by Liu et al. (Ref 10, 11) showed that selective formation of Al_2O_3 is a function of the coating grain size and that for the smallest grain size a compact alumina layer was formed on top of the coatings.

For thermal barrier applications, with a typical MCrAlY coating thickness of 100 to 150 μm, the sputtering technique is economically prohibitive (Ref 10, 11). MCrAlY coatings are typically deposited by vacuum plasma spray, low-pressure plasma spray, atmospheric plasma spraying, and recently, high-velocity oxyfuel (HVOF) spray (Ref 12, 13). These techniques can be used for different MCrAlY compositions. However, it is a technological challenge to control the grain size of the coating.

The original version of this article was published as part of the ASM Proceedings, *Thermal Spray 2003: Advancing the Science and Applying the Technology*, International Thermal Spray Conference (Orlando, FL), May 5-8 2003, Basil R. Marple and Christian Moreau, Ed., ASM International, 2003.

L. Ajdelsztajn, F. Tang, and **J.M. Schoenung,** Department of Chemical Engineering and Materials Science, University of California, Davis, CA 95616; **G.E. Kim,** Perpetual Technologies, Montreal, Quebec, Canada H3E 1T8; and **V. Provenzano,** National Institute of Standards and Technology, Gaithersburg, MD 20899. Contact e-mail: lajd@ucdavis.edu.

Table 1 Spraying parameters used to produce the NiCrAlY coatings

Gas	Pressure, MPa	FMR	GSF	Parameters	Setting
Air	0.69	40	5616	Powder feed rate (Ni-based substrate)	0.315 g/s
				Powder feed rate (Ni-based foil)	0.567 g/s
Fuel (C_3H_6)	0.69	43	1488	X-Y traverse speed (Ni-based substrate)	1.10 m/s
				X-Y traverse speed (Ni-based foil)	0.55 m/s
O_2	1.034	30	3410	Spraying distance	0.230 m

Note: FMR, flow meter reading; GSF, gas standard flow (mm^3/s)

The objectives of the present work were to produce, by the HVOF thermal spray process, a fine-grained coating structure using a nanocrystalline starting powder, and to study the oxidation behavior of these coatings. For comparison reasons, conventional NiCrAlY coatings were also synthesized using the HVOF thermal spray process.

2. Experimental Procedure

The material system studied in this work was a Ni-22wt.%Cr-10wt.%Al-1wt.%Y bond coat with a thickness of 102 μm, deposited on either a Ni-based alloy substrate or a Ni alloy foil (ASTM standard A 753-85 alloy type 4) using the HVOF thermal spray process. The feedstock powder was a commercially available NiCrAlY powder produced by Praxair Surface Technologies-Tafa (Ni-343) (Danbury, CT) with an average particle size of 28 μm. To obtain a nanocrystalline microstructure, the powder was mechanically milled at the rate of 180 rpm in a modified Union Process 01-ST (Akron, OH) attritor mill for 12 h under a liquid nitrogen environment. The liquid nitrogen was continuously introduced into the mill during milling to ensure complete immersion of the powders (the process is known as cryomilling or cryogenic milling) (Ref 14). Stainless steel balls with 6.4 mm diameter were used as the grinding media. The ball-to-powder weight ratio was 30 to 1.

A Sulzer Metco (Westbury, NY) Diamond Jet DJ 2700 HVOF thermal spray facility was used for thermal spraying of the NiCrAlY powders. The spraying parameters used to produce the coatings on the Ni-based alloy substrates and on the Ni alloy foils are summarized in Table 1. The surface of each substrate was grit-blasted before spraying. The surface of each foil was not grit-blasted, so a flat and smooth surface could be maintained. This type of surface provides poor adherence between the coating and the foil, facilitating the coating removal from the foil after spraying. This process results in a freestanding coating.

The number of spraying gun passes can be critical for the oxidation behavior due to the interpass oxidation present in HVOF coatings. To avoid this problem, the feed rate and the X-Y transverse speed values for the foil samples were different from those for the coating samples sprayed on the Ni-based substrate. These parameters were chosen so that a thick, freestanding coating could be produced with just one pass, avoiding the interpass oxidation effect. A detailed schematic of the freestanding sample preparation is shown in Fig. 1. The foil is attached to a steel substrate, and it is fixed in place by two fixtures. After spraying, the foil can be easily detached from the coating, leaving a freestanding coating sample.

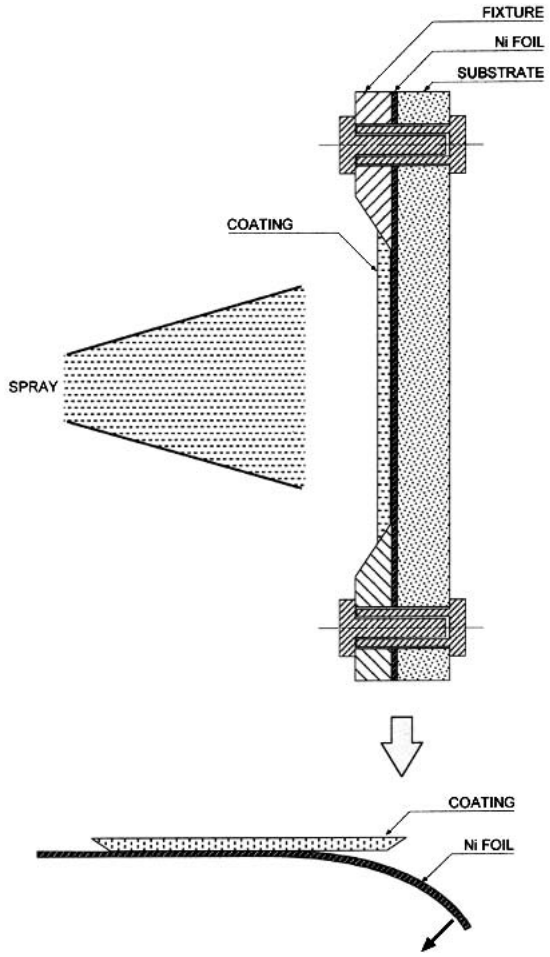

Fig. 1 Schematics of the free-standing specimen preparation. The Ni foil is attached to a steel substrate, and it is fixed in place by two fixtures. After spraying, the foil can be easily detached from the coating, leaving a freestanding coating sample.

After coating deposition, oxidation experiments were conducted in a high-temperature furnace at a constant temperature of 1000 °C in air atmosphere for different time periods (i.e., 4, 12, 24, and 48 h). Oxidation experiments were conducted on both the coatings deposited on the Ni-based substrates and the freestanding coatings, which had previously been removed from the foils. The surfaces, as well as the cross sections, of the heat-treated coatings were examined using scanning electron microscopy to identify the phases and morphology of the oxides formed during oxidation. For the freestanding coating, the analysis of the oxidized surface was carried out on the flat-bottomed surface, which was in contact with the foil during spraying. This procedure was adopted to minimize the effects of surface roughness on the oxide formation.

Secondary and backscattered electron images of the coatings were obtained, and energy dispersive spectroscopy (EDS) analysis was conducted using a Philips (Eindhoven, the Netherlands) XL30 FEG scanning electron microscope (SEM). Samples for SEM observation of the coatings were sectioned from a transverse section and were prepared by standard metallographic techniques.

3. Results and Discussion

3.1 Coating Characterization

The SEM images of the cross sections of the conventional and nanostructured NiCrAlY coatings obtained using the HVOF thermal spraying process on Ni-based substrates are shown in Fig. 2(a) and (b), respectively. In the nanostructured coatings, one can observe an increase in porosity when compared with that of the conventional coating. This can be explained by the different sizes of the agglomerates. After the as-received powder was cryomilled, the powder particle or agglomerate experienced a 150% increase in size, even though the microstructure of the material was reduced to a nanocrystalline regime. Using the same spray conditions for both powders (the as-received and the cryomilled), an increase in porosity content in the coating is expected due to the lack of melting or flattening of the large agglomerates, leaving gaps and voids in the coating (Fig. 2c).

The microstructure of the coatings (conventional and nanocrystalline) is characterized by two phases, γ (Ni-rich and Cr-rich) and β (Al-rich), as shown in Fig. 3 (a backscattered electron image of the conventional and the nanocrystalline coatings). The bright and dark areas correspond to the γ and β phases, respectively. According to XRD results, the γ′ phase (Ni_3Al) is also present in the coating microstructure. The grain size distribution in the conventional coating is relatively homogeneous throughout the cross section (1-1.5 μm). The final microstructure of the nanostructured coating has a fine grain structure that is characterized by a "multimodal structure," in which both nanocrystalline regions (approximately 75 nm from transmission electron microscope observation, Ref 15) and submicron grain regions (from 120-550 nm, Fig. 3) are observed.

In Fig. 4(a), one can observe in the backscattered SEM image that there are four dark layers in the coating cross section. According to EDS results, the dark layers are mainly composed of Al_2O_3, which, together with Y_2O_3, is the most kinetically favorable oxide to form. This interpass oxidation is a consequence of the high temperature that the coating experienced during the HVOF process. During the time between passes, the coating surface is still at a high temperature and, in the presence of air, starts to oxidize.

If the same coating is heat treated at 1000 °C for 24 h, a thickening of the interpass oxide layer can be observed (Fig. 4b). This process involves the Al diffusion out of the NiCrAlY alloy, and, as a consequence, a NiAl (β phase) depletion zone is developed (Ref 16) (Fig. 5). The depletion zone tends to increase in size with the continuation of the oxidation process. The same type of depletion zone is observed immediately below the TGO layer that forms on the top surface of the bond coat.

3.2 Oxidation Experiments

For the conventional coatings, samples that were heat treated at 1000 °C, the formation on the surface of a nonuniform alumina layer can be observed during the first hours of the heat treatment. After the 24 h heat treatment, this nonuniform layer manifests itself as mixed-oxide protrusions (Al_2O_3, NiO, and spinel phases such as $NiAl_2O_4$ and $NiCr_2O_4$) on top of the initial TGO layer (Fig. 6a). In Fig. 6(b), one can observe a detailed backscattered image of the mixed oxide layer shown in Fig. 6(a). On the basis of their atomic number in the backscattered imaging and EDS analysis, the dark layer close to the coating is Al_2O_3, the intermediate layer is rich in Cr, and the upper and brighter layer is rich in Ni.

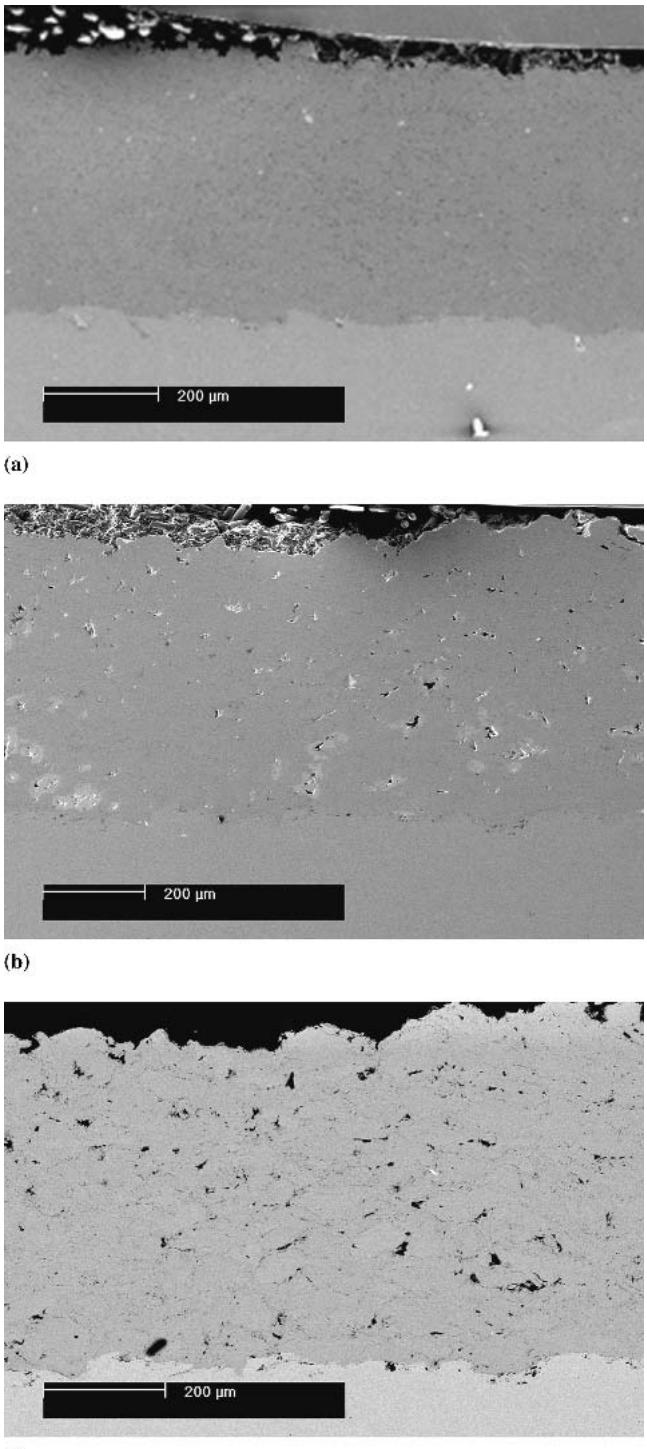

Fig. 2 Cross section of the (a) conventional and (b) nanostructured NiCrAlY coatings obtained using the HVOF thermal spraying process on Ni-based substrates. (c) Backscattered electron image of (b)

The morphology and the composition of the top TGO layer are crucial for the performance of TBC coatings. Although the oxidation of Y, Al, and Cr promotes a growth in the volume of the bond coat, the growth of NiO and some spinel phases can be more damaging because they exhibit a very high growth rate,

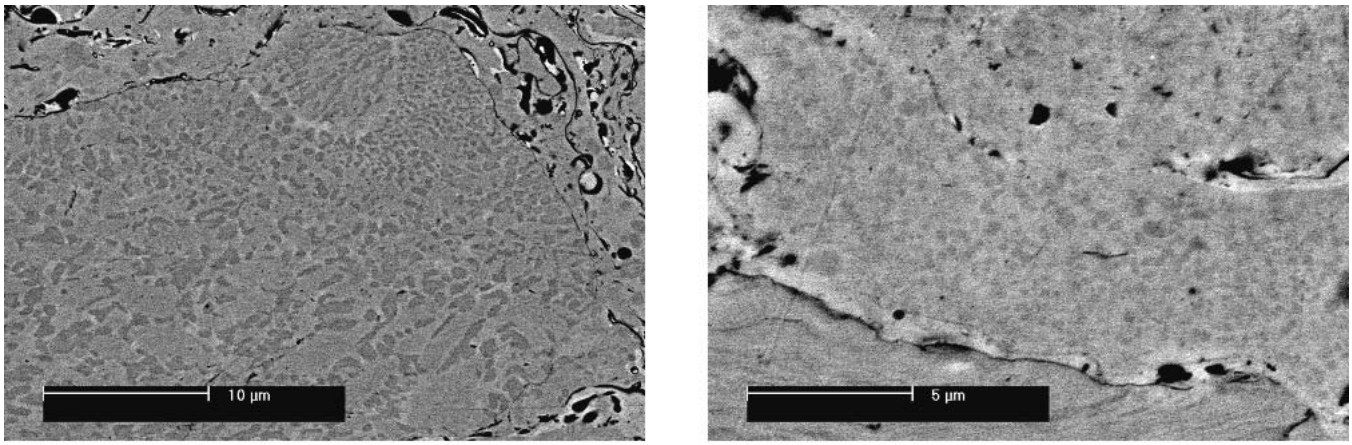

Fig. 3 SEM image of the cross section of the (a) conventional and (b) nanostructured NiCrAlY coatings showing the γ and β phases in the microstructure

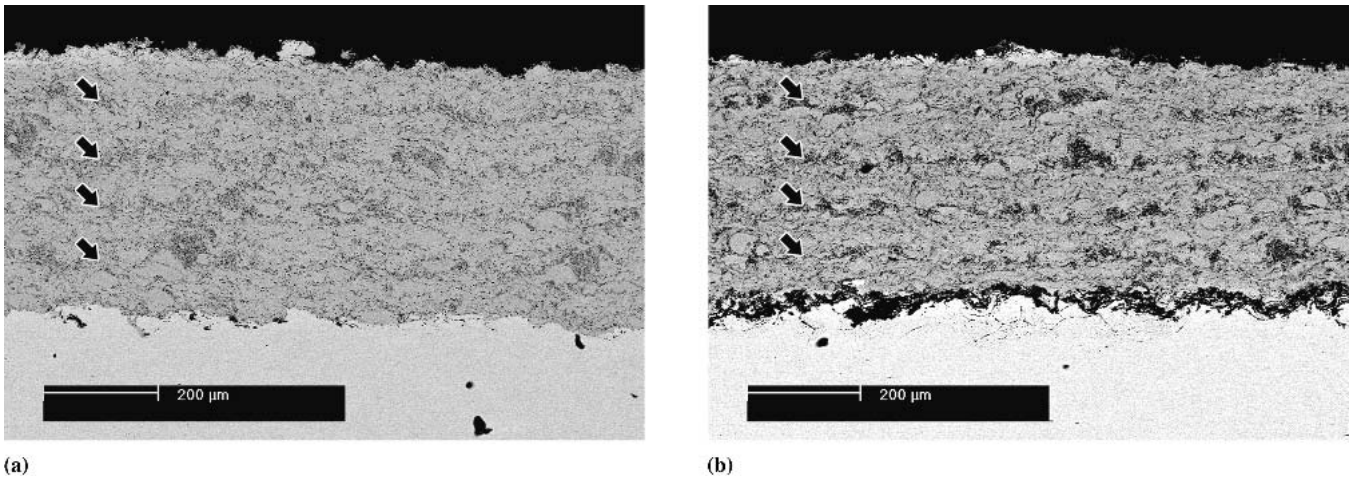

Fig. 4 (a) SEM image of the cross section of the conventional NiCrAlY coating showing the interpass oxidation layers after spraying. (b) The same coating after heat treatment for 24 h at 1000 °C

which rapidly increases the volume of the bond coat (Ref 17) and causes stresses in the YPSZ TBC, thus contributing to the initiation of the failure in the TBC system.

In contrast, the nanostructured coating presents a continuous TGO layer on its coating surface after oxidation (Fig. 7). According to EDS analysis, this layer consists mainly of Al_2O_3 (a slow-growing oxide, Ref 18). Very small traces of mixed oxide phases are observed on top of the alumina scale of the nanocrystalline coating after 48 h at 1000 °C. The difference in oxidation behavior can also be observed by viewing the top surface of the freestanding coatings (Fig. 8, 9).

One advantage of analyzing the freestanding coating sprayed with just one pass of the spray gun (besides the absence of species diffusing from the substrate to the interior of the coating during high-temperature experiments) is the fact that one can isolate the oxidation behavior process without the influence of a depletion zone originating next to an interpass oxide layer.

The top view of the surface of the conventional freestanding coating oxidized at 1000 °C for 12 h, which is seen in Fig. 8(a)

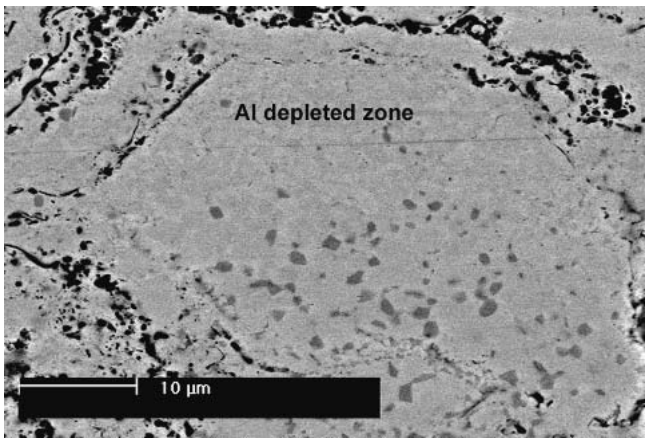

Fig. 5 Depletion zone in the conventional HVOF NiCrAlY coating next to an interpass oxide layer after heat treatment for 24 h at 1000 °C heat treatment

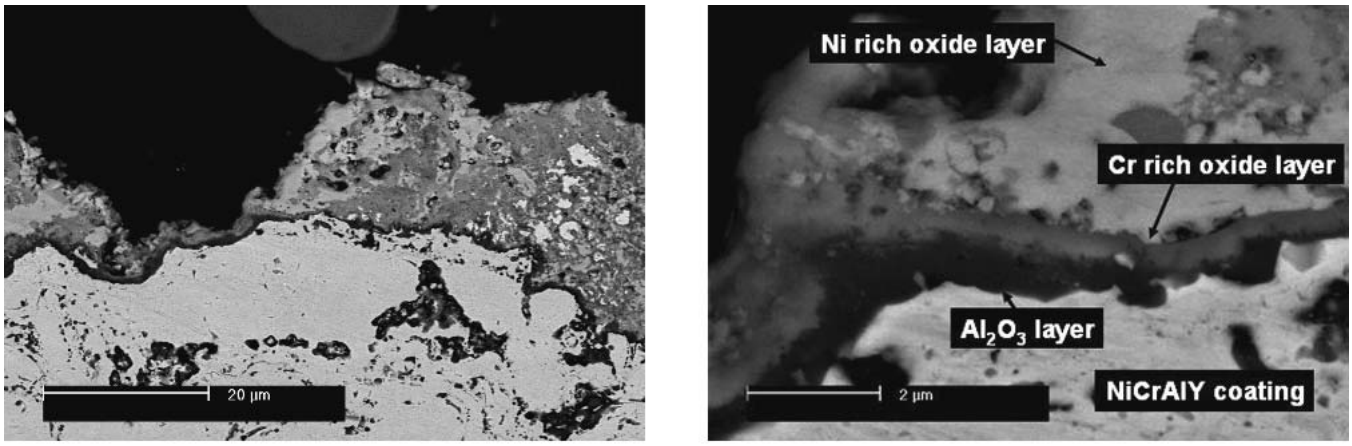

Fig. 6 (a) Formation of the TGO layer on the surface of the conventional HVOF NiCrAlY coating after heat treatment at 1000 °C for 24 h. (b) Higher magnification at the interface region

and (b), indicates the presence of oxide protrusions and the different morphologies of these constituents. The smoothed ridge structures at lower points of the surface, according to EDS analysis, correspond to the typical Al_2O_3 structure (Ref 19), and the polyhedral crystals at higher points on the surface correspond to the NiO structure (Ref 17). The same trend, but with a considerable increase in volume, can be observed in Fig. 8(c) and (d) after 24 h at the same temperature.

For the same oxidizing conditions, the surface of the nanostructured freestanding coating reveals a very different topography than the conventional coating. Figure 9 shows the evolution of the oxide scale with time (from 4 to 48 h of oxidation at 1000 °C). From the beginning of the oxidation process, the nanostructured coating presents a uniform and continuous Al_2O_3 layer, and the presence of other mixed oxide phases are not observed even after longer oxidation times (48 h). The transition with time from a morphology of smooth ridges to one with a dense oxide layer also can be observed. Some authors (Ref 20) refer to the morphology of smooth ridges as being characteristic of αAl_2O_3, which is present from the beginning of the oxidation process. Others (Ref 21-23) refer to this morphology as being characteristic of a metastable θAl_2O_3 phase that becomes α-Al_2O_3 with time, changing its morphology from this smooth ridge structure (Fig. 9a-d) to an equiaxed grain morphology, as observed in Fig. 9(g) and (h). Figure 9(e) and (f) show the presence of the two morphologies coexisting after 24 h of oxidation.

The different oxidation behavior is not completely understood and requires further investigation. Nevertheless, a simple experiment was conducted to confirm the importance of the nanocrystalline microstructure on the oxidation behavior of the nanostructured NiCrAlY bond coat. The surface of the oxidized (48 h) nanostructured coating was mechanically removed, and the thickness of the sample was reduced by half. The internal microstructure of the coating after 48 h of oxidation was no longer in the nanostructure regime (average grain size 15 3.2 μm). This newly polished surface of the coating was reoxidized for 12 h using the same conditions as in the previous experiments.

As is illustrated in Fig. 10, the new oxide layer that formed on the top surface of the reoxidized sample is composed primarily of an Al_2O_3 scale with some small regions where mixed oxides are present.

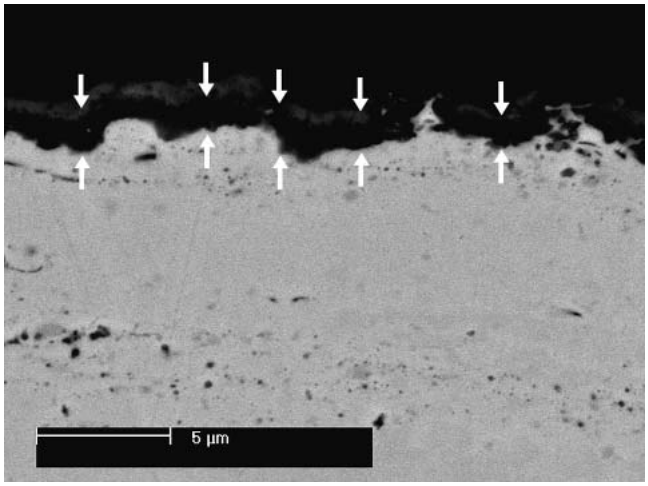

Fig. 7 Formation of the TGO (uniform Al_2O_3 layer) on the surface of the nanostructured HVOF NiCrAlY coating after heat treatment at 1000 °C for 24 h

The presence of these different oxides can be explained by observing the cross section of the coating below these regions (Fig. 11). Because the sample had already been oxidized for 48 h prior to the reoxidation, extensive interlamellar oxidation had occurred, and a depletion zone had formed in the proximity of the interlamellar region. Consequently, an insufficient number of Al atoms remained available for oxidation in these regions, leading to the formation of the mixed oxide regions observed in Fig. 10 and 11.

The fact that a preferential Al_2O_3 oxide layer was observed after the reoxidation experiment suggests that the refinement of the microstructure is not the only mechanism responsible for the preferential Al_2O_3 formation on the top surface. The powder exposure to cryomilling may modify the coating chemical composition and influence its oxidation behavior. Cryomilling is known to introduce oxides and nitrides that are finely dispersed within the powders (Ref 24). Further investigation is necessary to fully understand the oxidation mechanism presented in these nanostructured NiCrAlY coatings.

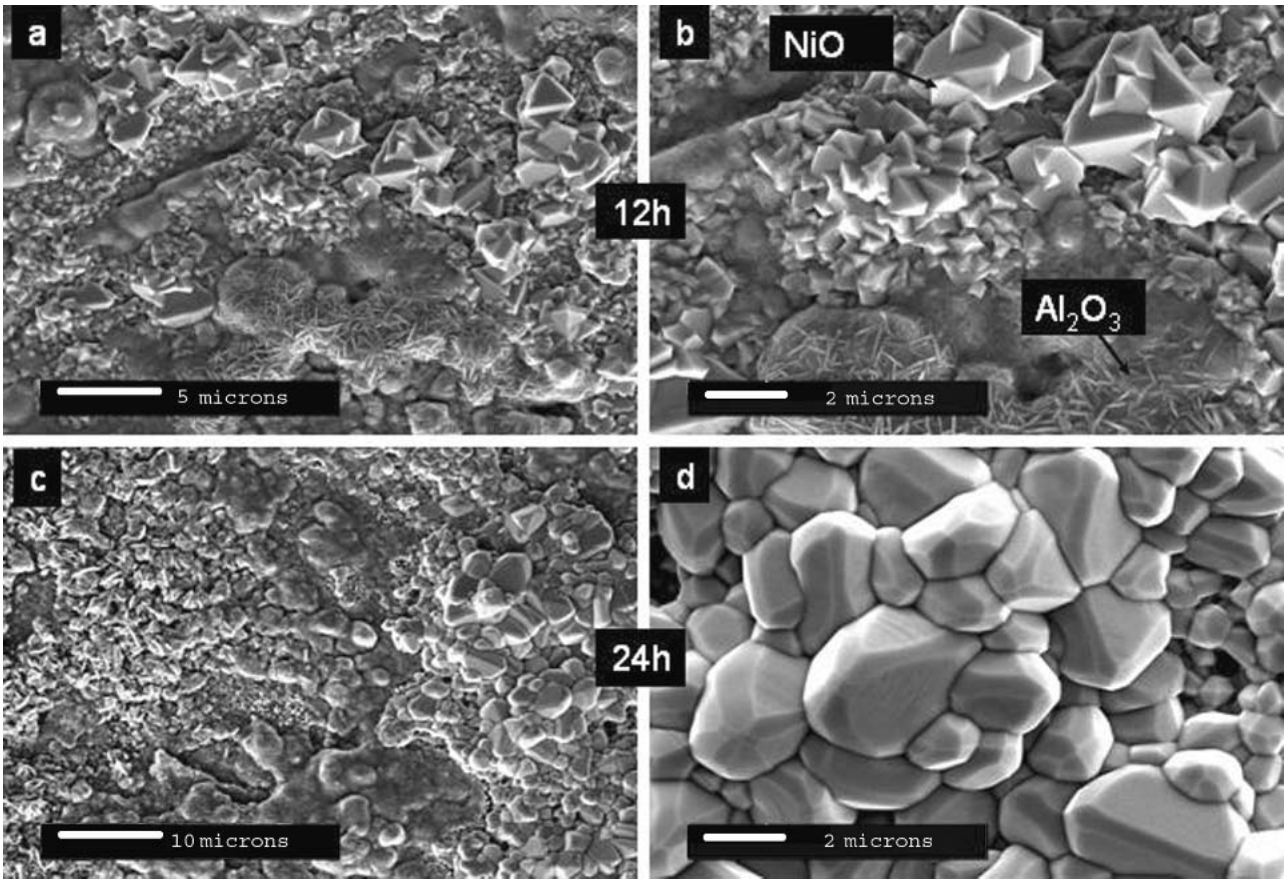

Fig. 8 Morphology of the oxide layer on the bottom surface of the conventional freestanding coating. (a) and (b) Oxidized at 1000 °C for 12 h. (c) and (d) Oxidized at 1000 °C for 24 h. Mixed oxides are observed at 12 h, and a considerable increase in oxide volume is observed after 24 h. In (d), one can see the coarsening of the NiO crystals with oxidation time.

4. Conclusions

The grain size refinement achieved with the cryomilling process was successfully used to produce nanocrystalline NiCrAlY powder and subsequent nanostructured bond coatings using the HVOF thermal spray process.

The oxidation behavior of both the conventional and nanostructured NiCrAlY coatings were investigated after heat treatments in air, at 1000 °C, for various times. After oxidation, the conventional coating exhibited a discontinuous alumina layer, as well as mixed oxides consisting of NiO and $Ni(Cr,Al)_2O_4$ spinels. For the nanostructured coating, oxidation led to the formation of a continuous alumina layer, without the presence of other mixed oxides.

The difference in oxidation behavior is a direct result of differences in microstructure and phase composition. One or both of the following mechanisms influences the oxidation kinetics. First, the nanocrystalline grain structure results in an increased grain-boundary area that could enhance aluminum diffusion. Second, the cryomilling introduces finely dispersed oxides that could promote the nucleation of alumina.

Longer oxidation tests (1000-3000 h) and cyclic oxidation tests (with an yttria-stabilized zirconium topcoat) are in progress to verify the influence of the nanocrystalline grain structure and/or the dispersed oxides on the oxidation behavior of coatings synthesized using the cryomilled NiCrAlY powder.

Acknowledgment

The authors are grateful to the Office of Naval Research (grant N00014-02-1-0213) for financial support.

References

1. J. He, G. Han, S. Fukuyama, and K. Yokogawa, Interfaces in a Modified Inconel 718 with Compact Precipitates, *Acta Mater.,* Vol 46 (No. 1), 1998, p 215-223
2. S. Shankar, D.E. Koenig, and L.E. Dardi, Vacuum Plasma Sprayed Metallic Coatings, *J. Met.,* Vol 33 (No. 10), 1981, p 13-20
3. J.T. DeMasi-Marcin and D.K. Gupta, Protective Coatings in the Gas Turbine Engine, *Surf. Coat. Technol.,* Vol 68-69, 1994, p 1-9
4. R.A. Miller, Thermal Barrier Coatings for Aircraft Engines: History and Directions, *J. Thermal Spray Technol.,* Vol 6 (No. 1), 1997, p 35-42
5. H.E. Evans and M.P. Taylor, Diffusion Cells and Chemical Failure of MCrAlY Bond Coats in Thermal-Barrier Coating Systems, *Oxid. Met.,* Vol 55 (No. 1-2), 2001, p 17-34
6. J.A. Haynes, M.K. Ferber, and W.D. Porter, Thermal Cycling Behavior of Plasma-Sprayed Thermal Barrier Coatings with Various MCrAlX Bond Coats, *J. Thermal Spray Technol.,* Vol 9 (No. 1), 2000, p 38-48
7. J.R. Nicholls, N.J. Simms, W.Y Chan, and H.E. Evans, Smart Overlay Coatings: Concept and Practice, *Surf. Coat. Technol.,* Vol 149 (No. 2-3), 2002, p 236-244
8. S.M. Meier, D.M. Nissley, K.D. Sheffler, and T.A. Cruse, Thermal Barrier Coating Life Prediction Model Development, *J. Eng. Gas Turb. Power,* Vol 114 (No. 2), 1992, p 258-263
9. Y.H. Sohn, J.H. Kim, E.H. Jordan, and M. Gell, Thermal Cycling of

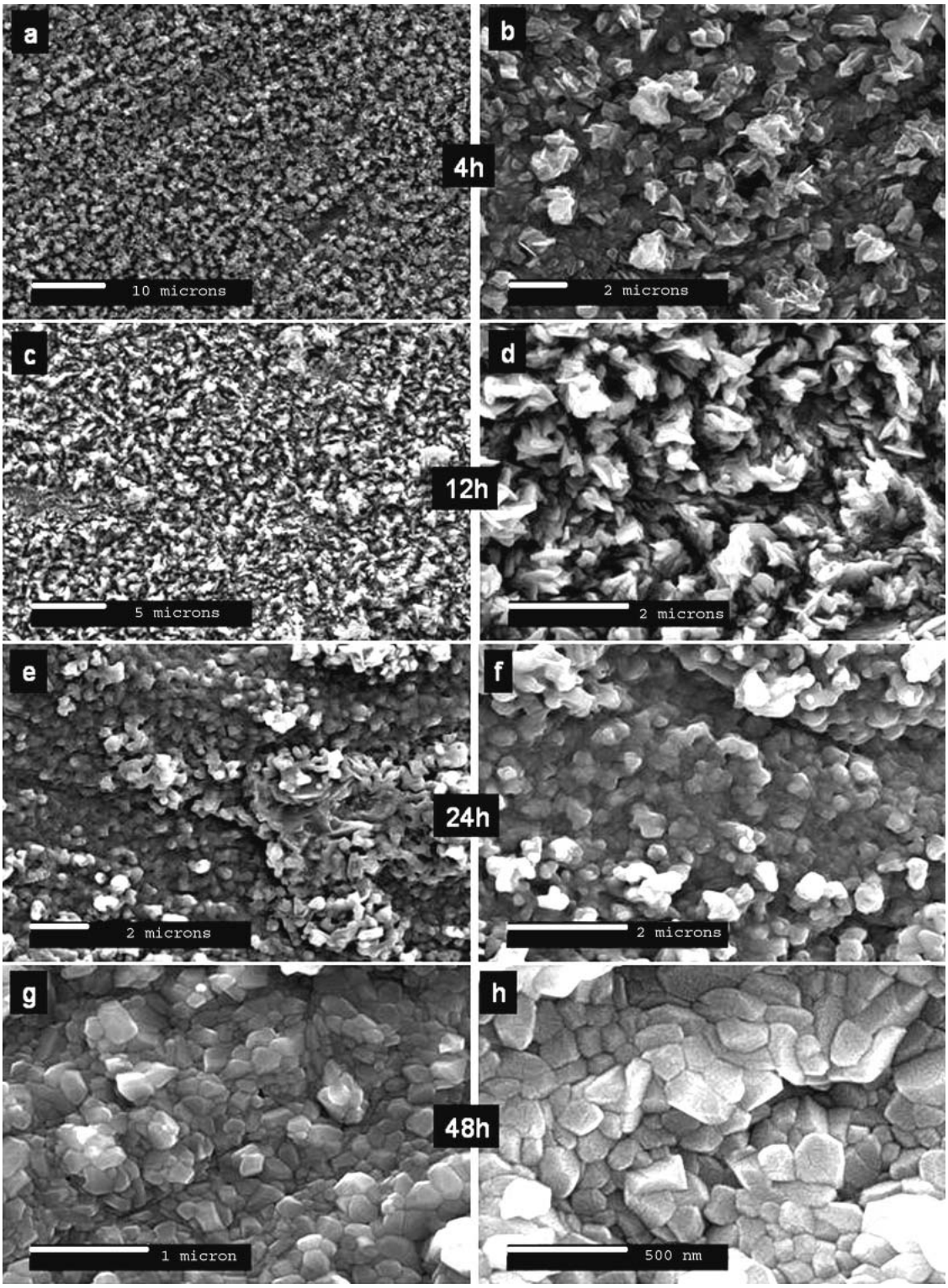

Fig. 9 Morphology of the oxide layer on the bottom surface of the nanostructured free-standing coating after oxidation at 1000 °C for various times. (a) and (b) 4 h. (c) and (d) 12 h. (e) and (f) 24 h. (g) and (h) 48 h. Mixed oxides are not observed. A transformation of the Al_2O_3 morphology with time is observed.

EB-PVD/MCrAlY Thermal Barrier Coatings: I. Microstructural Development and Spallation Mechanisms, *Surf. Coat. Technol.,* Vol 70 (No. 146-147), 2001, p 70-78

10. Z. Liu, W. Gao, K. Dahm, and F. Wang, The Effect of Coating Grain Size on the Selective Oxidation Behaviour of Ni-Cr-Al Alloy, *Scr. Mater.,* Vol 37 (No. 10), 1997, p 1551-1558

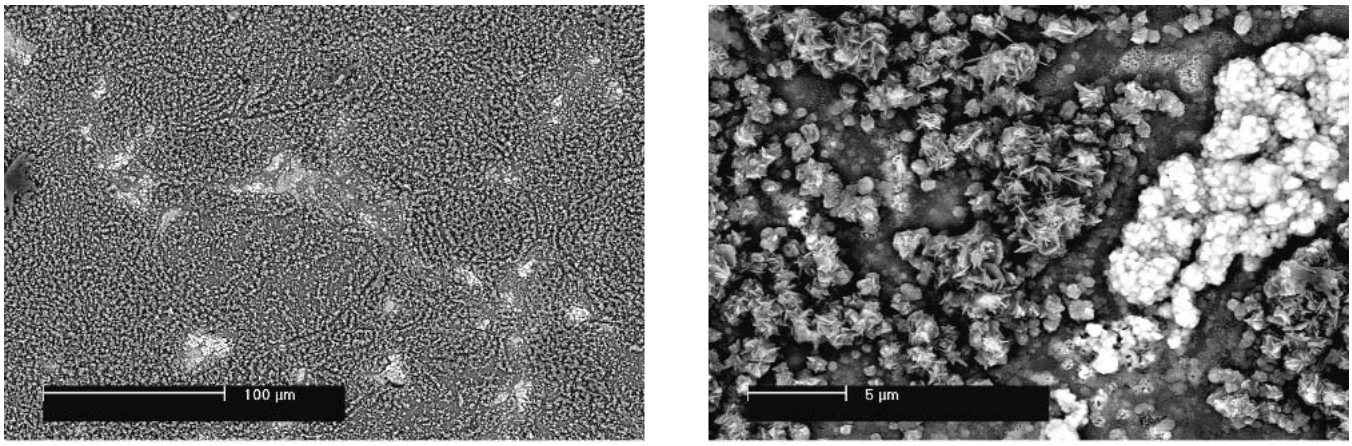

Fig. 10 Reoxidized nanostructured coating. (a) Top surface showing the dark alumina phase (darker regions) with some small mixed oxide regions (brighter regions). (b) Higher magnification at the interface between the alumina and the mixed oxides regions.

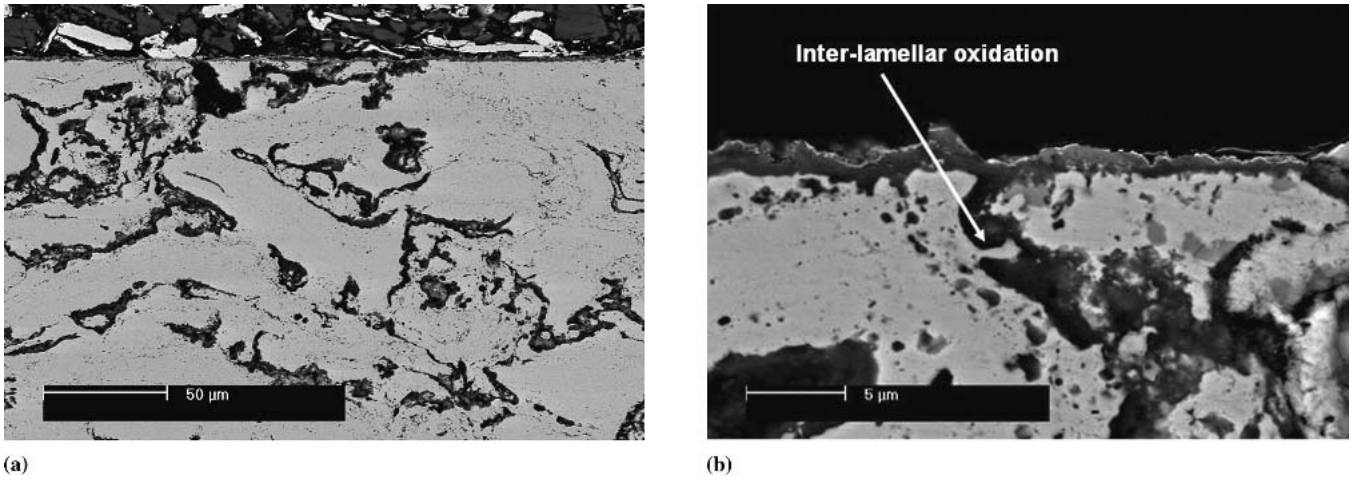

Fig. 11 (a) Cross section of the reoxidized nanostructured sample showing severe interlamellar oxidation. (b) Higher magnification showing the cross section beneath the mixed oxide layer.

11. Z. Liu, W. Gao, K. Dahm, and F. Wang, Oxidation Behaviour of Sputter-Deposited Ni-Cr-Al Micro-Crystalline Coatings, *Acta Mater.,* Vol 46 (No. 5), 1998, p1691-1700
12. W. Brandt, D. Toma, J. Krüger, H.J. Grabke, and G. Matthäus, The Oxidation Behaviour of HVOF Thermal-Sprayed MCrAlY Coatings, *Surf. Coat. Technol.,* Vol 94-95, 1997, p 21-26
13. W. Brandl., D. Toma, and H.J. Grabke, The Characteristics of Alumina Scales Formed on HVOF-Sprayed MCrAlY Coatings, *Surf. Coat. Technol.,* Vol 108-109 (No. 1-3), 1998, p 10-15
14. H.G. Jiang, M.L. Lau, V.L. Tellkamp, and E.J. Lavernia, *Handbook of Nanostructured Materials and Nanotechnology: Synthesis and Processing,* H.S. Nalwa, Ed., Academic Press, 2000, p 159-213
15. L. Ajdelsztajn, J.A. Picas, G.E. Kim, F. L. Bastian, J.M. Schoenung, and V. Provenzano, Oxidation Behavior of HVOF Sprayed Nanocrystalline NiCrAlY Powder, *Mater. Sci. Eng., A,* Vol A338 (No. 1-2), 2002, p 33-43
16. A. Rabiei and AG. Evans, Failure Mechanisms Associated with the Thermally Grown Oxide in Plasma-Sprayed Thermal Barrier Coatings, *Acta Mater.,* Vol 48 (No. 15), 2000, p 3963-3976
17. X. Wu, D. Weng, Z. Chen, and L. Xu, Effects of Plasma-Sprayed NiCrAl/ZrO_2 Intermediate on the Combination Ability of Coatings, *Surf. Coat. Technol.,* Vol 140 (No. 3), 2001, p 231-237
18. D.F. Susan and A.R. Marder, Oxidation of Ni–Al-Base Electrodeposited Composite Coatings: II. Oxidation Kinetics and Morphology at 1000°C Marder, *Oxid. Met.,* Vol 57 (No. 1-2), 2002, p 159-180
19. D. Toma, W. Brandl, and U. Koster, The Characteristics of Alumina Scales Formed on HVOF-Sprayed MCrAlY Coatings, *Oxid. Met.,* Vol 53 (No. 1-2), 2000, p 125-137
20. D. Toma, W. Brandl, and U. Koster, Studies on the Transient Stage of Oxidation of VPS and HVOF Sprayed MCrAlY Coatings, *Surf. Coat. Technol.,* Vol 120-121, 1999, p 8-15
21. J.C. Yang, E. Schumann, I. Levin, and M. Ruhle, Transient Oxidation of NiAl, *Acta Mater.,* Vol 46 (No. 6), 1998, p 2195-2201
22. G. Muller, G. Schumacher, and D. Straub, Oxide Scale Growth on MCrAlY Coatings after Pulsed Electron Beam Treatment, *Surf. Coat. Technol.,* Vol 108-109 (No. 1-3), 1998, p 43-47
23. D. Strauss, G. Muller, G. Schumacher, V. Engelko, W. Stamm, D. Clemens, and W.J. Quaddakers, Oxide Scale Growth on MCrAlY Bond Coatings after Pulsed Electron Beam Treatment and Deposition of EBPVD-TBC, *Surf. Coat. Technol.,* Vol 135 (No. 2-3), 2001, p 196-201
24. R.J. Perez, B. Huang, and E.J. Lavernia, Thermal Stability of Nanocrystalline Fe-10 wt.% Al Produced by Cryogenic Mechanical Alloying, *Nanostruct. Mater.,* Vol 7 (No. 5), 1996, p 565-572